Copyright © 2011 by ABCM

INVESTIGATING THE PERFORMANCE OF A MEMS CAPACITIVE ACCELEROMETER USING FINITE ELEMENT ANALYSIS

André da Costa Teves, andreteves@gmail.com
School of Engineering, University of São Paulo, 05508-010, Sao Paulo/SP – Brazil

Janderson Rocha Rodrigues, jrr@ita.br
Aeronautics Institute of Technology, 12228-900, Sao Jose dos Campos/SP – Brazil

Angelo Passaro, angelo@ieav.cta.br
Institute for Advanced Studies, 12228-001, Sao Jose dos Campos/ SP – Brazil

Emilio Carlos Nelli Silva, ecnsilva@usp.br
School of Engineering, University of São Paulo, 05508-010, Sao Paulo/SP – Brazil

Carlos Fernando Rondina Mateus, mateus@ieav.cta.br
Institute for Advanced Studies, 12228-001, Sao Jose dos Campos/SP – Brazil

Luis Carlos Sandoval Góes, goes@ita.br
Aeronautics Institute of Technology, 12228-900, Sao Jose dos Campos/SP – Brazil

Abstract. *This paper focuses on studying the different physics involved in the operation of a novel capacitive MEMS (Micro-Electromechanical Systems) bulk-micromachined accelerometer, using Finite Element Analysis (FEA). A typical design for such sensors consists of a large proof mass connected to surrounding structures by elastic beams. The mass moves proportionally to the externally applied acceleration; the movable electrode is sandwiched between two fixed plates and the displacement is measured by the change in the differential capacitance. Static displacement due to gravity, resonant frequencies, electrostatic force, pull-in point and squeezed-film gas damping are taken into account in a multiphysics approach. Moreover, a parametric analysis is done by varying several parameters such as gap, mass and beam's dimensions, thickness and gas pressure and their effect on sensitivity and dynamic response are assessed. This study is part of the project AcelerAD, funded by FINEP, which objective is to establish the full development cycle (design, simulation, electronics, packaging and testing) of a MEMS capacitive accelerometer for applications in embedded systems such as aircraft, rockets, and satellites.*

Keywords*: MEMS, capacitive accelerometer, simulation, finite element method, multiphysics*

1. INTRODUCTION

Micro-Electro-Mechanical Systems (MEMS) is an enabling technology that allows one to design complex devices in a micrometer scale. Through the use of microfabrication techniques, adapted from the semiconductor industry, the integration of movable structures, sensors, actuators and electronics is accomplished, making possible to implement complete miniaturized systems (Madou, 2002). Because MEMS devices are manufactured using batch fabrication techniques, unprecedented levels of functionality, reliability and sophistication can be placed in a small silicon chip at a relatively low cost.

Accelerometers are among the top sellers MEMS devices nowadays (Kaajakari, 2009), this is because they are used in a wide range of applications: in the automotive industry, they are used as crash sensors for air bag deployment and in active suspension systems; in several consumer applications, such as the latest generation of video games and cell phones, they enable enhanced user interface; high performance accelerometers are used in the arms industry and in aerospace applications for missile guidance, inertial navigation, unmanned vehicles, among others.

They are actually one of the simplest types of MEMS sensors, since they consist of little more than a seismic mass, also known as proof mass, and flexible beams, working as springs. The external acceleration is translated to displacement of its proof mass that can be measured by various detection schemes, some of the most relevant are capacitive, piezoelectric, piezoresistive, resonant and optical (Yazdi et al., 1998). Capacitive accelerometers have become more popular due to the relatively ease of fabrication, high sensitivity, good dc response and noise performance, low temperature sensitivity and low-power consumption (Lui *et al*., 2007).

They are usually implemented by surface or bulk-micromachining technology. The former generally uses a comb-like structure as sensing electrode, the thickness of the deposited layer and hence the proof mass is small, causing limitations on the performance of the accelerometers. On the other hand, in bulk micromachined devices, due to the presence of a large proof mass, higher resolution and greater sensitivity is achievable.

This work describes a capacitive bulk-micromachined accelerometer, which is fabricated using KOH etch. The device is modeled in a commercial finite element software and several physics involved in its operation, such as static

displacement due to gravity, resonant frequencies, electrostatic force, pull-in point and squeezed-film gas damping, are considered in the analysis. This study is part of a project, which objective is to establish the full development cycle (design, simulation, electronics, packaging and testing) of a MEMS capacitive accelerometer for applications in embedded systems such as aircraft, rockets, and satellites.

This paper is organized as follows. In Section 2, the basics of the capacitive accelerometer are presented. The computational model is discussed in details in section 3 and the results are presented in section 4. Finally, section 5 provides the concluding remarks and points to future developments.

2. THE CAPACITIVE ACCELEROMETER

A simple analogy to the z-axis accelerometer studied is this paper is illustrated in Fig. 1. When voltage is applied over the structure, the two fixed plates and the movable mass form a differential capacitor with the same initial gap *d*. The spring constant *k* corresponds to the intrinsic stiffness of the beams that connect the movable plate to the rest of the structure.

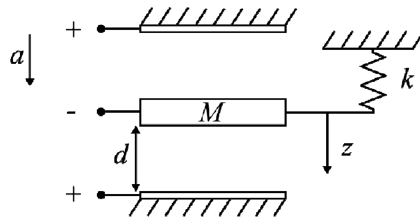

Figure 1 – Schematic of the accelerometer.

The resulting force acting on the movable plate is given by:

$$F_R = F_{ett,bot} + F_g - F_{ett,top} - F_k \quad (1)$$

where $F_{ett,bot}$ and $F_{ett,top}$ are the electrostatic force due to the top and bottom electrodes respectively, F_k is the elastic force and F_g is the inertial force. Substituting the values for each component in Eq. (1) results in:

$$F_R = \frac{\varepsilon A V^2}{2(d-z)^2} + Ma - \frac{\varepsilon A V^2}{2(d+z)^2} - kz \quad (2)$$

where ε is the dielectric constant, A is the area of the plates, V is the applied voltage, M is the mass of the movable plate, z is the vertical displacement and a is the external acceleration. As the external load or the voltage increases, the electrostatic force $F_{ett,bot}$ increases faster than the other forces and the movable plate will snap down, this is known as pull-in point. Estimating this parameter is very important for a successful design of electrostatic sensors and actuators. A simple expression for the pull-in point (Kaajakari, 2009) is obtained by deriving Eq. (2) to obtain a measure of the stiffness of the system:

$$\frac{\partial F_R}{\partial z} = \varepsilon A V^2 \left(\frac{1}{(d-z)^3} + \frac{1}{(d+z)^3} \right) - k \quad (3)$$

If $\partial F_R / \partial z$ becomes positive the system is unstable: a small positive movement δz results in positive force that increases z even further. The pull-in point can be calculated by finding when $\partial F_R / \partial z = 0$:

$$\varepsilon A V^2 \left(\frac{1}{(d-z)^3} + \frac{1}{(d+z)^3} \right) - k = 0 \quad (4)$$

The solution to Eq. (4) is found graphically for the dimensions used in our accelerometer, as plotted in Fig. 2.

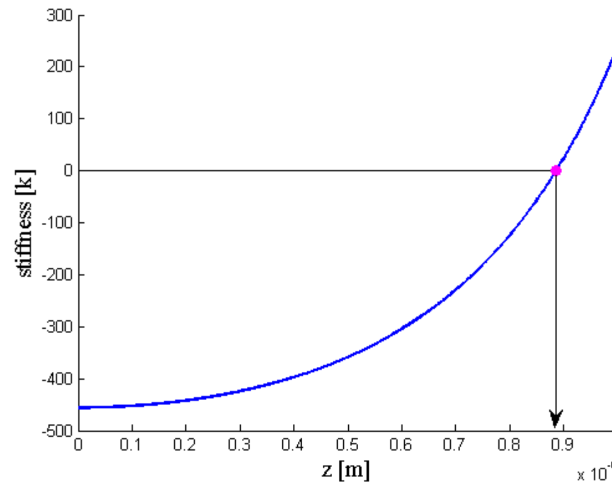

Figure 2 – Pull-in point is calculated graphically.

As can be noted from Fig. 2, the displacement of the movable mass is limited to 0.88µm for the 2µm gap used in our design.

For simplicity the effect of damping was not accounted for in the previous analysis. Known as squeeze film damping, it is particularly important in MEMS because the effect of surface forces on microscale is very significant. For a detailed review of the topic the reader is referred to Bao and Yang (2007).

The dimensions of the accelerometer studied are in this paper are presented in Tab. 1 and Fig. 3. A large proof mass (middle plate) is connected to surrounding structures by elastic beams. The mass moves proportionally to the applied acceleration (input signal); the movable electrode is sandwiched between two fixed plates and the displacement is measured by the change in capacitance (output signal). The three silicon wafers used have (100) orientation and silicon oxide (in green) is used as insulation between the layers. The middle layer is patterned using KOH solution, which etchs the monocrystalline silicon anisotropically, i.e., with different etching rate, according to the orientation of the silicon's crystal planes, resulting in a 54.74º wall angle, (Dziuban, 2006).

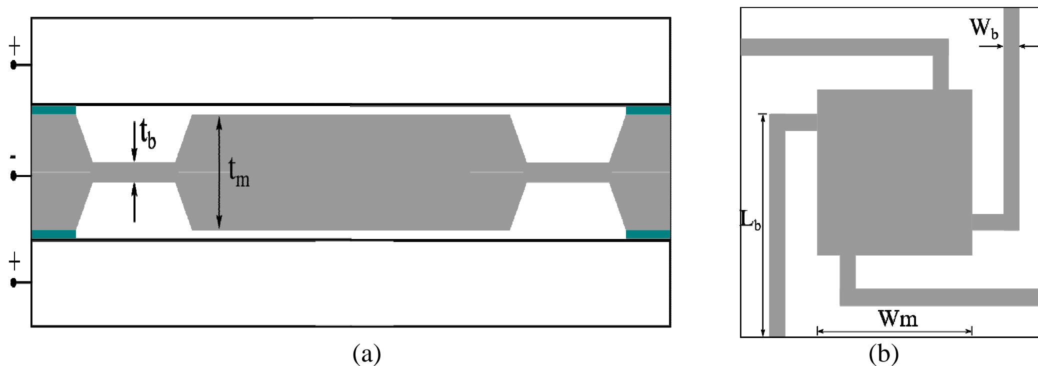

(a) (b)

Figure 3 – Cross-section (a) and top view (b) of the accelerometer.

Table 1. Geometric parameters of the accelerometer simulated.

Description	Symbol	Value[µm]
Width of the seismic mass	W_m	2000
Thickness of the seismic mass	t_m	380
Length of the beam	L_b	2820
Width of the beam	W_b	177
Thickness of the beam	t_b	55

3. COMPUTATIONAL APPROACH

The design presented in Fig. 3 is modeled in a commercial finite element software. Two different models with increasing level of details are developed. The first is a three dimension model including only structural mechanics analysis and is applied to the study of static displacement due to gravity and resonance frequencies. Due to

computational limitations, a less computationally expensive 2D model is built to consider more complex problems involving different physics, such as electrostatic and squeeze-film damping. The two models are presented in Fig. 4.

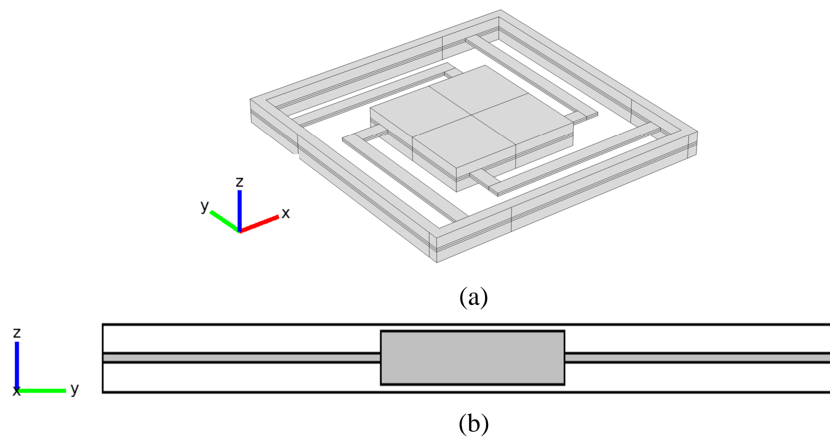

Figure 4 – Model of the accelerometer in 3D (a) and 2D (b).

The 3D model is discretized in 56,826 tetrahedral elements, whereas the 2D model contains 48,620 triangular elements.

The material of the movable plate and beams is silicon with the following properties: density $\rho = 2330\ kg/m^3$, Young's modulus $E = 131\ GPa$ and poisson ratio $\upsilon = 0.27$. Note that in contrast to the first model, the air inside the device is included in 2D and it will be used in the damping and electrostatic analysis presented in section 4. The values used for the permittivity of the air is $\varepsilon = 8.85\ pF/m$, the dynamic viscosity is $\mu_D = 22.10^{-6}\ Pa.s$ and the mean free path is $\lambda = 70\ nm$.

For all structural mechanics analysis the beam is clamped in its extreme. It should be mentioned that the length of the beam in the second model is adjusted to match the mechanical behavior of the 3D model.

Furthermore, for simplicity, the angle resulting from the fabrication process using KOH is not considered in any model.

4. RESULTS

4.1. Static displacement due to gravity and sensitivity

First of all, the displacement of the proof mass due to a vertical acceleration of 1g (self-weight) is calculated to be 56nm as shown in Fig. 5(a), which is much smaller than the 2µm gap between the two plates. The displacement is magnified by a factor of 10.000. Figure 5(b) displays the associated von Mises stress distribution, clearly showing that the material is in the elastic regime and well below the yield strength of silicon, 7GPa (Kovacs, 1998). Even if the external acceleration is increased to the level (roughly 35g) where the displacement of the mass reaches the maximum of 2µm, the von Mises stress is still well below the yield strength of material. As stated earlier and is now clear in Fig. 5, the device is fixed by its rim.

Next, the influence of the geometry of the arms in the value of the sensitivity of the accelerometer is evaluated. This is a particularly important study for MEMS devices as they are inherently subjected to dimensional variations due to the fabrication process. In capacitive accelerometers, the sensitivity (S) is defined as the relative change of capacitance per unit of acceleration and is given by (Ramos, 1997):

$$S = \frac{1}{f_1^2}\frac{9.8}{4\pi^2}\frac{C_{act}}{gap} \tag{5}$$

where f_1 is the first resonance frequency and C_{act} is the active capacitance.

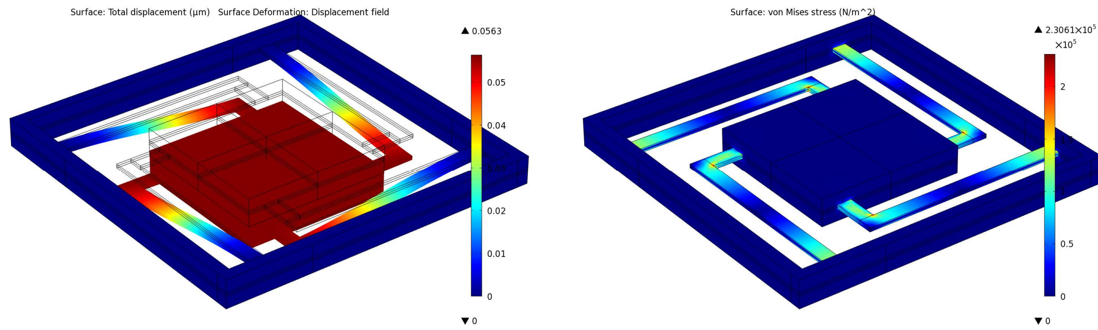

Figure 5 – Static displacement (left) and von Mises stress (right) due to gravity.

Following the work done by Alvarez et al. (2009), a parametric analysis with the thickness (x_1) and the width (x_2) of the L-shaped beams varying respectively from 50-60μm with steps of 2μm and from 180-240μm with steps of 20μm was performed. The sensitivity response surface based on a full quadratic regression model is plotted in Fig. 6. The polynomial function S' obtained is the following:

$$S' = 7.246 - 0.158x_1 - 0.014x_2 + 9.621\cdot10^{-4}x_1^2 + 1.241\cdot10^{-4}x_1x_2 + 1.094\cdot10^{-5}x_2^2 \quad (6)$$

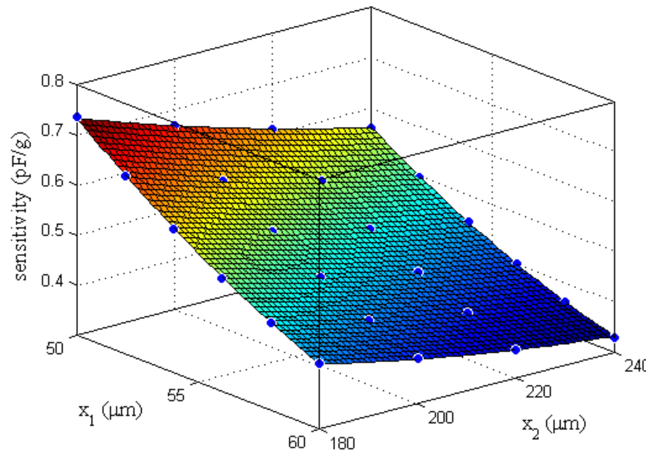

Figure 6 – Surface plot of sensitivity vs (x_1,x_2).

The model has an adjusted R^2 of 0.997, that is, 99.7% of the variation is explained by the model. The most important linear effect is the thickness of the beams and as its value increases, the value of the sensitivity decreases. The second order terms are at least two orders of magnitude smaller than the others. By analyzing Fig. 6, it is possible to say that even in the worst case, when x_1=60μm and x_2=240μm, the sensitivity still achieves values bigger than 0.3pF/g, which means that the design is sufficiently robust.

4.2. Resonant frequencies

Based on the 3D model, the first six resonance frequencies are calculated and the results are presented in table 1. The first two eigenmodes are presented in Fig. 7.

Table 1. Resonant frequencies for the accelerometer

#	1	2	3	4	5	6
Hz	2116	4919	4920	36877.4	38879	46120

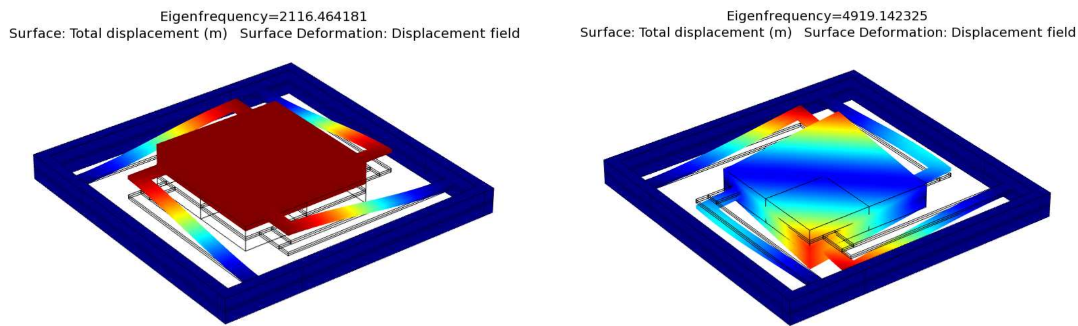

Figure 7 – First (left) and second (right) resonance frequencies.

Due to the highly symmetrical design, the second and third eigenfrequencies, as well as the fourth and fifth, correspond to the same vibration mode, the difference in their pair of values is caused by numerical truncation and irregularities in the finite element mesh. It is worth mentioning that from the fourth to the sixth resonance frequency, the result is an order of magnitude larger than previous ones, which means that in normal operation they should not affect the device performance.

Furthermore, it is interesting to note that the value of the first frequency is very close to the value obtained analytically:

$$f_1 = \frac{1}{2\pi}\sqrt{\frac{k}{M}} = 2105,3 \text{ Hz} \tag{7}$$

where k is the spring constant of the system formed by four beams and M is the mass of the movable plate. The agreement of the results validates the analytical approach as a reasonable initial approximation.

4.3. Electrostatic analysis and pull-in point

As stated earlier, the electrostatic physics is only included in the 2D model. An electric potential of 5V is applied to the top and bottom electrodes, the proof mass is grounded (0V) and the beam is clamped in its extreme. Figure 8(a) illustrates the electric potential distribution in the entire structure. Figure 8(b) is zoomed view of the electric potential distribution in the gap region.

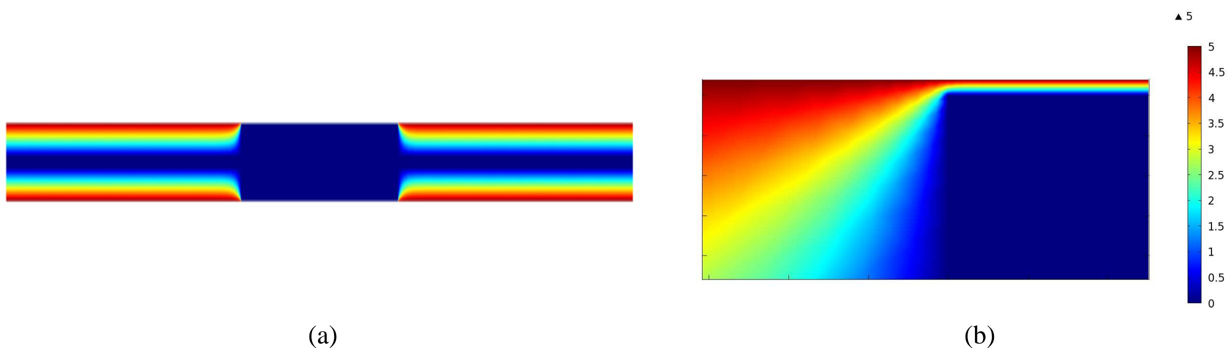

(a) (b)

Figure 8 – Electric potential distribution.

Next, a parametric study is performed by varying the external acceleration acting on the movable structure from 1g to 10g, in order to assess the changes in the capacitance (Fig. 9) and the variation of the gap (Fig. 10).

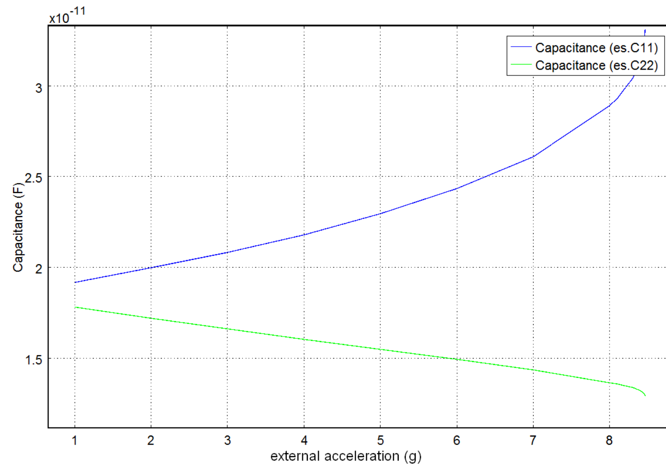

Figure 9 – Variation of the capacitance in the upper (green) and lower (blue) sets of electrodes.

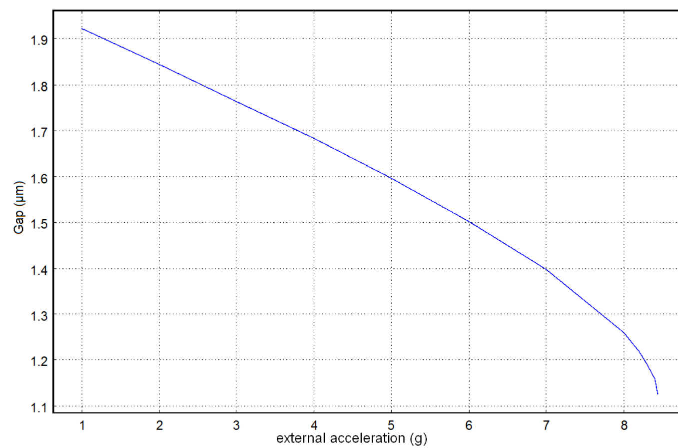

Figure 10 – Variation of the bottom gap with the external acceleration.

Both capacitances are of the order of tens of pF and, as expected, they show opposed patterns of variations.

The study is run up to 10g but starting at 8.45g the software starts to present problems of convergence and the solution is finalized, which can be explained by the high non-linearity associated with the pull-in effect. Examining Fig. 10, the instability happens at approximately 0.85 µm and thus coincides with the pull-in point calculated analytically in section 2. Once again, the agreement of the two values validates the analytical approach as a reasonable initial approach.

4.4. Squeeze film damping

For MEMS devices based on proof mass, the film damping due to the presence of air inside the device's cavity is a major issue, since this effect dominates the damping of the system and thus substantially affects its frequency response. To study the system response to this phenomenon, a time-dependent analysis is performed in the 2D geometry using a built-in thin film model.

Figure 11 shows the oscillatory behavior of the system when subjected to an external acceleration of 1g in the vertical direction at t = 0s. A parametric analysis varying the internal pressure from 3Pa to ambient pressure (10^5 Pa) is performed. Figure 12 shows the intensity of the damping forces (N) in the upper (F_{top}) and lower (F_{bot}) faces of the movable plate when the internal pressure is 300Pa.

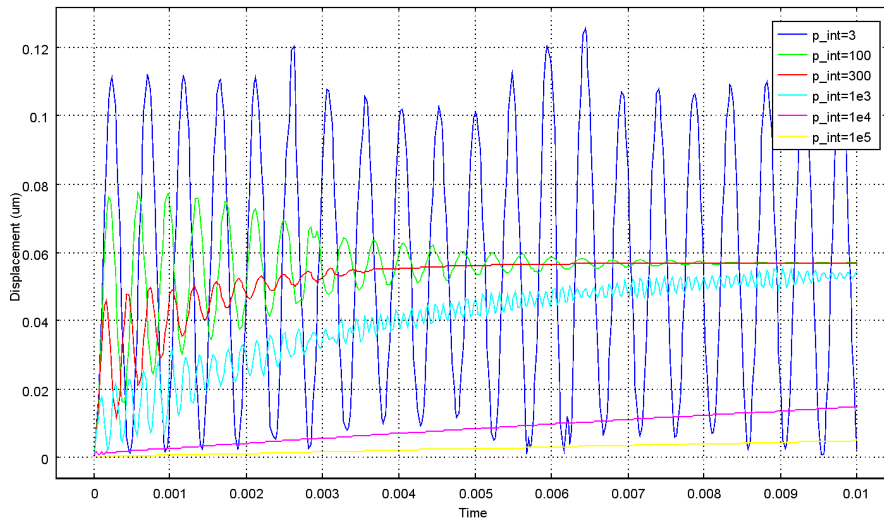

Figure 11 – Squeeze film damping for different internal pressures.

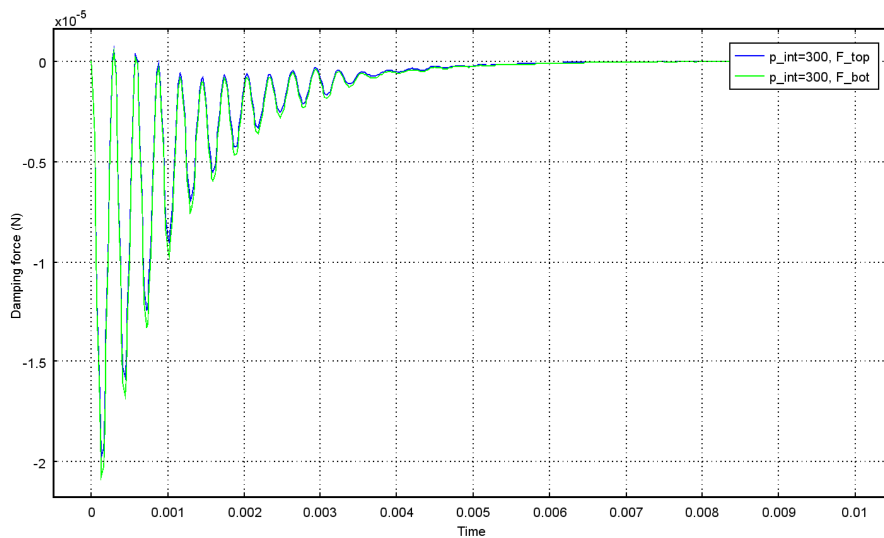

Figure 12 – Damping forces acting on the moving mass.

For an internal pressure of 3Pa the system is oscillatory and for internal pressure bigger than 10^4Pa the system takes a long time (more than 30ms) to reach steady state, which corresponds to a displacement of approximately 57nm for 1g. Both patterns are not desirable in the operation of accelerometers.

From Fig. 11, one can say that the optimal response time would occur with an internal pressure of 100-1000Pa. Thus, a new parametric analysis is performed, this time varying the internal pressure with steps of 200Pa starting at 400Pa (Fig. 13).

Based on the two parametric studies, it is possible to say that the optimal value for the internal pressure is somewhere between 300-500 Pa.

Finally, the influence of the air damping in the first resonance frequency is evaluated by performing a frequency domain analysis. The resulting Bode plots are shown in Fig.14 for two different scenarios. The first considers only the intrinsic material damping given by Rayleigh model (damping factor $\xi = 0.1$) and the second considering air damping with internal pressure of 500Pa. In both cases, the study swept from 1 to 10^5Hz.

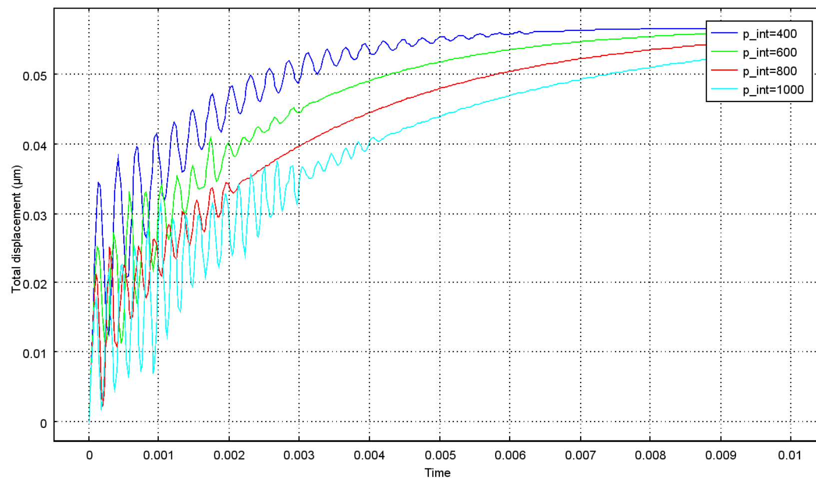

Figure 13 – Second study using a smaller pressure range.

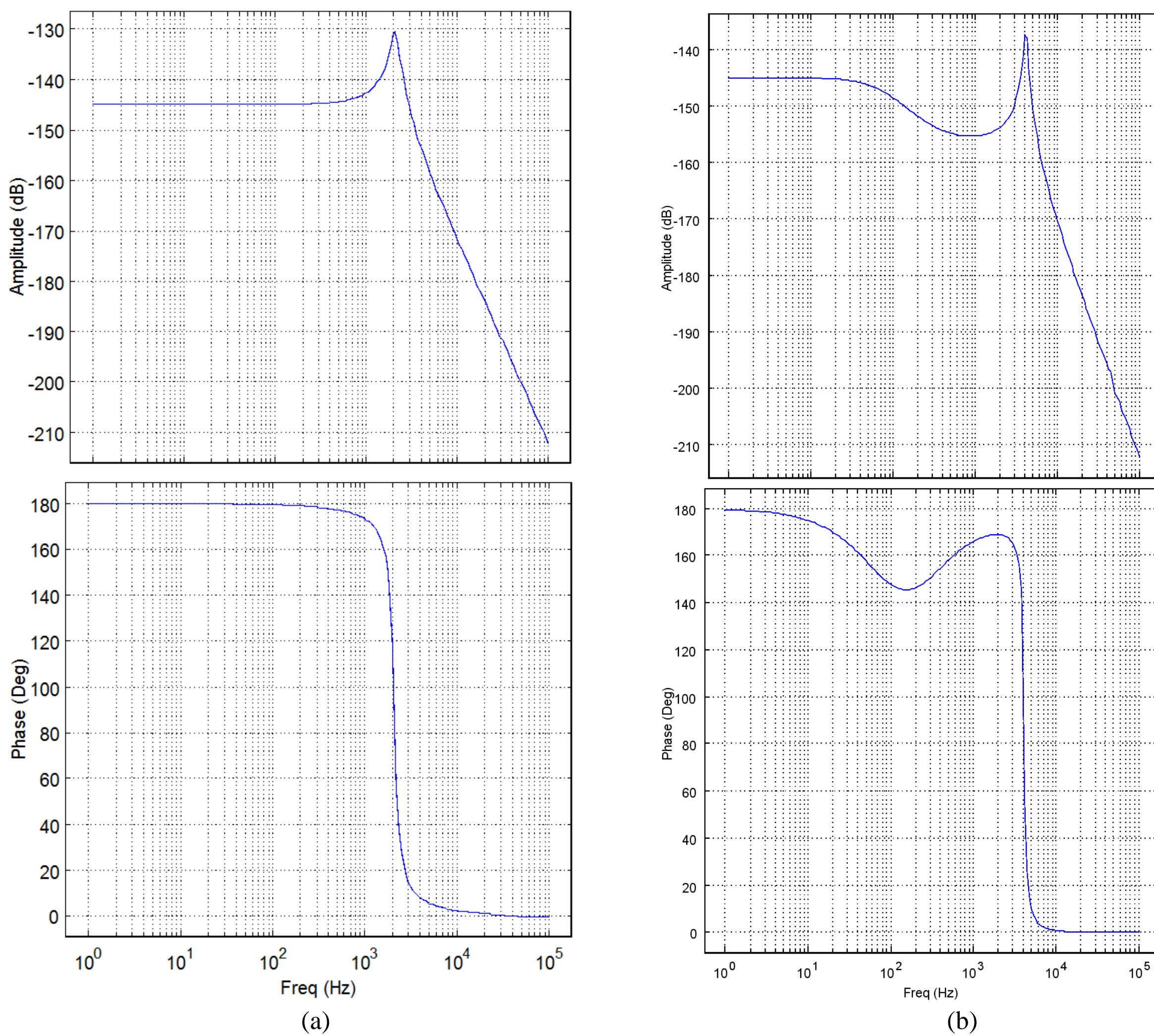

Figure 14 – Bode plots for (a) intrinsic material damping and (b) air damping.

By observing the plots from Fig. 14 it is possible to conclude that the presence of the air shifted the first resonance frequency to approximately 4 kHz. However, this increase does not mean performance improvement since the bandwidth (flat frequency range) actually decreased. The shape of the curve obtained in this analysis is consistent with that seen in Bao & Yang (2007).

Copyright © 2011 by ABCM

5. CONCLUSIONS

In this study, a capacitive bulk-micromachining accelerometer has been analyzed using the finite element method. Several important parameters such as displacement with varying input accelerations, response time, resonance frequencies and pull-in point were calculated. The last two show very good agreement with simple analytical calculations. In short, the results confirm that the device is applicable to its intended use in embedded systems such as aircrafts, rockets, and satellites.

More detailed models, considering the angles resulting from the KOH etch and more complex multiphysics interactions are the next planned steps. This will require more computational resources but should give us a better idea of the accelerometer in real operational conditions.

In parallel to this study, other parts of the development cycle of the micro-accelerometer are being considered by the AcelerAD project team, such as analytical models including static mechanical analysis and damping, fabrication and optimization.

6. ACKNOWLEDGEMENTS

This work was supported by FINEP (Brazilian Agency for Funding of Studies and Projects) under grant 01.09.0395.00 through the project AcelerAD. The fourth author also acknowledges the financial support of CNPQ (National Council for Research and Development) under grant 303689/2009-9.

7. REFERENCES

Alvarez, M.J., Gil-Negrete, N., Ilzarbe, L., Tanco, M., Viles, E. and Asensio, A., 2009. "A computer experiment application to the design and optimization of a capacitive accelerometer. ". Applied Stochastic Models in Business and Industry, Vol. 25, pp. 151–162.

Bao, M. and Yang, H., 2007. "Squeeze film air damping in MEMS", Sensors and Actuators A, Vol.136 pp. 3–27.

Dziuban, J.A., 2006, “Bonding in Microsystem Technology”, Ed. Springer, Netherlands.

Kaajakari, V., 2009. "Practical MEMS", Small Gear Publisher.

Kovacs, T. Gregory, 1998. "Micromachined Transducers Sourcebook", McGraw-Hill.

Lui, X., Zhang, H., Li, G., Chen, W. and Wang, X., 2007, “Design of Readout Circuits Used for Micro-machined Capacitive Accelerometer”, Proceedings of the 2nd IEEE International Conference on Nano/Micro Engineered and Molecular Systems, Bangkok, Thailand, pp. 537–541.

Madou, J. Mark, 2002. "Fundamentals of Microfabrication: the science of miniaturization", CRC Press.

Ramos, J., 1997. “Sensitivity enhancement in lateral capacitive accelerometers by structure width optimsation”, Electronic letters, Vol.33, pp. 384-386.

Yazdi, N., Ayazi, F. and Najafi, K., 1998. “Micromachined inertial sensors”. Proceedings of the IEEE, Vol. 86, No. 8, pp.1640-1659.

7. RESPONSIBILITY NOTICE

The authors are the only responsible for the printed material included in this paper.